Journal of Thermal Analysis and Calorimetry, Vol. 61 (2000) 661–679

A STUDY OF TEMPERATURE-MODULATED DIFFERENTIAL SCANNING CALORIMETRY WITH HIGH-RESOLUTION INFRARED THERMOGRAPHY

R. Androsch[1*], *M. Pyda*[1], *H. Wang*[2] *and B. Wunderlich*[1**]

[1]Department of Chemistry, University of Tennessee, Knoxville, TN 37996-1600
and Oak Ridge National Laboratory, Chemical and Analytical Sciences Division, Oak Ridge
[2]Oak Ridge National Laboratory, High Temperature Materials Laboratory, Oak Ridge, TN, USA

(Received January 14, 2000)

Abstract

Temperature gradients within the sample and furnace in temperature-modulated differential scanning calorimetry (TMDSC) are studied for a power-compensation calorimeter of the Perkin Elmer type. The temperature measurements were made with a high-speed, high-resolution infrared camera. Differences between programmed and actual temperature amplitudes are determined as a function of sample thickness for a sawtooth modulation with up to 48 K min^{-1} heating and cooling rates. Phase angles have been established, and the effect of open and sealed sample pans has been analyzed. A simple one-dimensional description of the observed effects is made and a three-dimensional one is suggested based on a model available in the literature.

Keywords: differential scanning calorimetry (DSC), infrared thermography, phase angle, temperature gradient, temperature-modulated differential scanning calorimetry (TMDSC)

Introduction

Differential thermal analysis (DTA), differential scanning calorimetry (DSC), and temperature-modulated differential scanning calorimetry (TMDSC) are based on the temperature measurement of a sample and a reference which are both placed in closely similar environments and heated or cooled under controlled scanning conditions [1]. For all three instruments, the quantitative determination of calorimetric information relies on the existence of correct temperature gradients that govern the heat-flux rates. The difference between reference and sample temperatures, ΔT, is usually recorded *vs.* the programmed sample temperature, the measured sample temperature, or time. The ΔT is proportional to the differential heat-flow rate after a

* Present address: Institute of Material Science, Martin-Luther-University, Halle-Wittenberg, Geusaer Str., 06217 Merseburg, Germany.
** Author for correspondence: Department of Chemistry, University of Tennessee, Knoxville, TN 37996-1600, USA.

1418–2874/2000/ $ 5.00
Akadémiai Kiadó, Budapest

proper calibration of the DSC which can also be designated as a scanning, isoperibol twin-calorimeter. The actual calorimeters are the reference and sample materials in their enclosures which frequently consist of sealed aluminum pans.

In this paper, we describe the first experiments of measurement of temperatures with an infrared camera. During typical TMDSC runs, this method allows a direct study of the three main temperature gradients which are found between the heater and sample-temperature sensor, the sensor and the surface temperature of the furnace which is also equal to the bottom temperature of the sample, and the bottom and the top temperatures of the sample. Knowledge of temperature gradients is essential for precision measurements in TMDSC. The approach we have chosen is the direct measurement of the temperature-time-profile at the bottom of the pan and at the surface of samples of different thickness using high-speed and high-resolution infrared thermography [2] and comparison with the recorded sample temperature from the sample-temperature sensor. The experimental data are then analyzed with a simple one-dimensional heat-flow model, and a suggestion is made, how the three-dimensional case can be handled, based on literature data.

About temperature gradients and steady state

A simple model has in the past been sufficient for the mathematical description of DSC measurements. It is based on the assumptions that steady state exists throughout the calorimeter and only a negligible temperature gradient persists within the sample, and radiation losses and convection is negligible [1]. The differential heat-flow rate can then be used for quantitative characterization of the thermal behavior of the sample. One can derive the heat capacity, C_p, which represents the heat, Q, needed to change the temperature, T_s, of the sample ($C_p=dQ/dT_s$) and any latent heats, $L(=\Delta Q)$ arising from physical transitions and chemical reactions. The measurement of T_s is realized by sensors in close proximity of the sample calorimeter. Well-defined heat-conduction-paths characterize the twin calorimeter.

After a change in the scanning rate of the temperature within a DSC, the reference and sample temperatures exponentially approach a new steady state. If an overall steady state is reached, all points in the calorimeter change their temperature at the same rate with lags in ΔT which are proportional to the appropriate heat capacities:

$$\Delta T=\frac{qC_p}{K} \tag{1}$$

where q is the heating rate in K min^{-1} which may have values as high as 40 K min^{-1}, and K is the Newton's law constant in J K^{-1} min^{-1}. The time-constants governing the approaches to the steady states depend on the calorimeter and sample properties (such as heat capacity, thermal conductivity, and contact resistance to heat transfer in both, the sample and reference calorimeters).

For heat capacity measurements with the standard DSC, one need not be concerned about any of the temperature gradients and their temperature-dependence, since for measurement one waits for steady state, and the remaining gradient within

the sample can be kept to be negligible. At steady state, any temperature gradient within the sample makes the measurement uncertain over the temperature range of the gradient. Depending on the conditions of measurement this gradient is typically ±0.1 K. The heat capacity of a polymer, such as liquid polyethylene, however, changes by only 0.12% per kelvin at 400 K, so that one is safely outside the common error limit of heat capacity measurement by DSC (about ±3% [3]). A minor correction due to the different heating rates in reference and sample calorimeters which arise from the changes of C_p with temperature can be made without need of a further calibration [1], but is usually also neglected.

The temperature-modulated DSC, in contrast to the standard DSC, continually alters its rate-of-change of temperature. This gives rise to perpetually changing steady states and temperature gradients. The conditions needed for standard DSC could be approached by TMDSC when using a sinusoidal temperature modulation of rather long period, p, and a sufficiently low amplitude, A_{T_s}. The conditions are a maintenance of steady state and a negligible temperature gradient within the sample throughout the modulation cycle. Heat capacity measurements were then carried out by determining the amplitudes of the modulated sample temperature, A_{T_s}, and the heat flow rate, A_{HF}, the latter being proportional to ΔT, the temperature difference between reference and sample calorimeter (T_r–T_s) [4]:

$$C_p = \frac{A_{HF}}{A_{T_s}} \frac{1}{\omega} K(\omega) \tag{2}$$

where ω is the modulation frequency (=2π/p) and $K(\omega)$ is a dimensionless correction factor. If the sample and reference pans are identical in mass and there is no inherent asymmetry between the two calorimeters, one can derive that the expression for $K(\omega)=[1+(C_r\omega/K)^2]^{0.5}$, with C_r representing the heat capacity of the reference calorimeter and K, the above described Newton's law constant. In actual applications, however, $K(\omega)$ is usually chosen as a calibration constant, evaluated by measurements with a calibrant (often a single-crystalline sapphire) using the identical reference calorimeter, frequency and modulation amplitude. It must be noted, however, that as soon as temperature gradients appear within the sample and steady state is not reached, this type of calibration is not applicable, as will be discussed below. In this case the sample and the sapphire calibration runs require different values of $K(\omega)$. The asymmetry is corrected by evaluation of the deviation of the heat capacity from zero when two empty, identical calorimeters are being measured, taking into account the phase lags of the two empty calorimeters. Initially the limits of Eq. (2) were explored only empirically [4].

Developing TMDSC for multiple frequencies, as generated by sawtooth modulation and different types of temperature control, it became necessary to reassess Eq. (2). First, it was shown that, in contrast to Eq. (1) for the standard DSC, it is not a necessary condition that steady state is reached when using Eq. (2), as long as the calorimeter responds linearly to the induced rates of temperature change (see, for example [5]). For example, in heat-flux calorimeters the response to changes in tempera-

ture can be fully described by the Fourier equation of heat flow ($\partial T/\partial t = k\nabla^2 T$, where k is the thermal diffusivity, and ∇^2, the Laplacian operator). This equation is a linear, homogeneous differential equation and several overlapping thermal events lead to additive solutions [1, 6]. The correction factor $K(\omega)$ for the more general case without steady state and not-negligible temperature gradients was then written as $[1+(\tau\omega)^2]^{0.5}$ [7], where the constant τ can be determined empirically from measurements on the same sample using a number of different frequencies [7–11]. Each sample and varying experimental condition yields a different τ.

To obtain highest precision with TMDSC [10] one may also have to cover the frequency range when steady state is not reached, which is for most presently used calorimeters and measurement conditions a modulation period less than 60 s for sinusoidal modulation [4] and 150 s for sawtooth modulation (for an amplitude of about 1.0 K) [7]. The customary Fourier transformation [12] for data reduction from the time domain to the frequency domain, requires then, besides the calibrations of the temperature and heat-flow rate, and correction for asymmetry, the evaluation of a calibration function unique for the run condition, compensating the different approaches to steady state of the sample and reference (τ is dependent on frequency, amplitude, sample mass, thermal conductivity, thermal contact-resistance, and the temperature gradient within the sample) [7–10].

In contrast to the rather straight-forward determination of the heat capacity, the characterization of latent heat effects might become a more serious problem. Under equilibrium conditions, any first-order transition of a one-component system, such as melting of a pure substance, occurs at a thermodynamically defined and constant temperature. A temperature gradient within the sample will be distorted by the latent heat being absorbed at different points of the sample at different times. Even more complicated are such latent-heat effects under irreversible conditions. Details have been studied for many years using special methods for the standard DSC [1], and are now also developed for the temperature-modulated DSC [5]. In particular, when analyzing materials with relatively sharp transitions, and when applying rather small modulation amplitudes, for instance 0.05 K, and a low underlying heating rate, the sample might undergo a latent-heat involving transition in a layer surrounded by material which cannot undergo the same transition due to a temperature lag relative to the oscillating temperature. In the melting region, the cylinder of a sample in a TMDSC experiment may, thus, consist of an inner core of crystal surrounded on all sides by melt which changes its boundaries periodically with the modulation while slowly advancing to the center, seriously distorting the measured signal as found at the bottom of the calorimeter [5].

This problem of temperature gradients within the sample when using temperature-modulated DSC is well recognized, and was discussed on the basis of theoretical calculations by Buehler *et al.* [13, 14]. The authors presented an analytical solution for the temperature gradient within the sample considering thermal conductivities. The mathematical model is a cylinder, like a DSC pan, where heat is introduced at the top and side surfaces, the heat flow at the bottom into the sample was set to zero. According to the calculation of a typical temperature-modulation on a poly(ethylene

terephthalate) disc with a thickness of 0.74 mm and the modulation parameters amplitude 1 K, and period 60 s, the difference between the amplitudes between the top and bottom of the sample was calculated to be 0.3 K; the same drop of the amplitude was measured in the axial direction [13]. It will be shown in the discussion section of this paper that this model, which does not adequately describe a standard TMDSC, can be modified based on the present results without any further computation to a good representation of the sample and reference calorimeters.

Experimental

Calorimetry

For the investigation, a power-compensating Perkin Elmer DSC 7 was used. Despite using in this work only one specific type of calorimeter, it can be recognized that many of the conclusions apply also to the various heat-flux calorimeters, when appropriate changes are made. The sample holder of the DSC 7 was changed from its standard configuration as is illustrated in Fig. 1a, to have access with the infrared camera to the sample and reference furnaces. The dry box and the aluminum cover were removed. The planar aluminum block was covered by a single, large sapphire disc to avoid unnecessary heat losses to the environment. Additionally, the two furnaces were covered by small sapphire discs, replacing the original platinum lids. The sapphire discs are transparent in the 0.3–4 μm infrared region, and drop to about 60% transmittance by 5 μm. The thermography makes use of the 3–5 μm wavelength for the direct, non-contact temperature measurement. The calibration with the uniform surfaces, described below, and with all sapphire discs in place corrects for any spectral absorption and change in sensitivity of the IR camera. A typical experiment is illustrated in Fig. 1b for an open, half-filled sample calorimeter at 423 K.

The TMDSC also was calibrated in this changed configuration with the sapphire discs in place. The standard procedure consists of correction of the sensor temperature, T_s, using the onset of the melting process of indium and tin, a calibration of the energy with the heat of fusion of indium, and an adjustment of program temperature, T_p, and sensor temperature. All temperature-modulated experiments were performed quasi-isothermally at 423 K. This temperature was selected to guarantee the programmed cooling rate in absence of additional cooling devices, which would cause condensation on the sample and reference holders and likewise affect the temperature measurement with the infrared camera. The amplitudes and periods in the sawtooth-type modulation experiments were 0.5, 1.0, 2.0, and 4.0 K, and 20, 30, 40 and 60 s, respectively. The figures displaying the results are marked, where necessary, with obvious abbreviations to indicate the mode of the experiment in question, separated by periods, commas, or underlines (iso=quasi isothermal experiment; 423=experimental set-temperature of 423 K; per20=period of 20 s or other value; amp05=modulation amplitude of 0.5 K or other value; IR=temperature indicated by the infrared camera; TS=sensor temperature as measured by the calorimeter; TP=programmed temperature as set for the calorimeter; difference=normalized difference between IR or TS

and TP; top, bottom = temperature indicated by the infrared camera at the top or bottom of the sample – for the procedure, see Fig. 1b; covered=measured in a closed aluminum pan; uncovered=measurement in an open aluminum pan; lag=measured phase lag between the top and bottom of the sample; 1 mm=sample thickness of 1.00 mm, or other value).

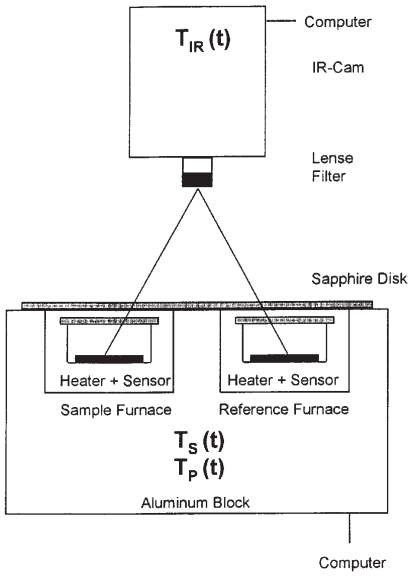

Fig. 1a Schematic of the experimental setup based on the Perkin Elmer DSC 7

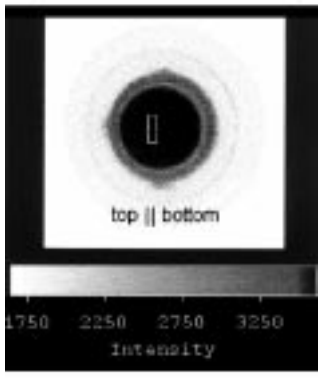

Fig. 1b Image of the sample-furnace at 423 K, including a 1mm thick polymer sample of poly(ethylene-*co*-octene) (on the left, not covered). The right half of the sample pan is empty. The rectangle marks the area that is used for the integration of the IR intensity

Samples

Experiments were performed using a commercial polyester film [poly(ethylene terephthalate)], poly(ethylene-*co*-octene) [24 mass% 1-octene, M_w=78.000 Da], and poly(butylene terephthalate) [POCAN B 1305™, Bayer AG, M_w=40.700 Da]. The polyester film had a thickness of about 0.1 mm. Several layers were stacked into the pan, permitting the evaluation of the sample-mass/thickness effect, including a sample which covered only half of the calorimeter (Fig. 1b). Whereas the polyester film was semi-crystalline at 423 K, the poly(ethylene-*co*-octene) was completely melted. The effect of thickness of the latter sample was analyzed for thicknesses of 0.175 and 1.0 mm, and that of the semi-crystalline poly(butylene terephthalate) for 1.0 mm. Beside the estimation of temperature gradients as a function of modulation parameters, we tried to minimize systematic errors and artefacts by using various samples which differ in thermal properties, mass, thickness, and structural state. A change in structure, for instance, could easily result in deformation of the sample on the initial heating to 423 K due to changes in internal stress or orientation, and alter in this way the temperature profile by changing the thermal resistance. Samples were prepared such that the infrared camera had simultaneous access to the bottom of the pan and the top of the sample as illustrated in Fig. 1b.

Infrared camera

The instrument used was Amber's Galileo high-speed, high-sensitivity infrared camera with a 256×256 pixel resolution and a 12 bit digital intensity resolution, using an indium antimonide focal-plane array as detector. The camera was operated in the sequence mode, taking snapshots with a frequency of 2 Hz and an integration time of approximately 1.0 ms. The maximum number of frames during one scan was limited to 140, *i.e.*, the maximum scanning time was 70 s. A neutral density filter ND1 was used to adjust the intensity. All objects exposed to temperature measurements were sprayed with graphite or an ultra-flat, black paint to equalize and maximize absorption and emission of infrared radiation from all surfaces studied. The sample-to-detector distance was adjusted to get a spatial resolution of about 0.5 and 0.2 mm/pixel, respectively. Using the lower resolution of 0.5 mm/pixel, data from the sample and the reference furnace could be obtained simultaneously. The intensity signal of the camera was calibrated before each experiment on the basis of known temperature differences. Absolute temperature measurements were not performed. The intensity was averaged over a reproducible area, as shown, for example by the rectangle in Fig. 1b.

Figure 2 shows a typical calibration experiment to adjust the intensity scale of the camera to a temperature scale. The IR camera was focused on the top of the crimped pan in the sample furnace and the intensity signal of the infrared camera was recorded *vs.* the isothermally kept DSC, as characterized by the program and sensor temperatures. The data were gathered in 5 K increments between 403 and 433 K, covering the entire temperature interval used in the quasi-isothermal modulation experiments. The data were fitted into a straight line which is an acceptable approximation within the small temperature interval covered in Fig. 2. The slope of the fit in this par-

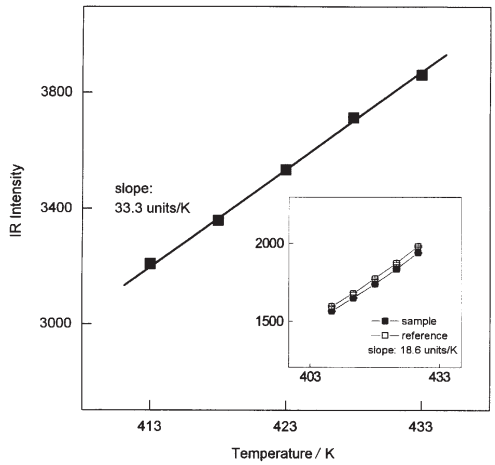

Fig. 2 A typical calibration for the infrared camera at two furnace-to-detector distances. The insert shows data recorded at a larger distance, allowing simultaneous detection of the reference and sample furnaces

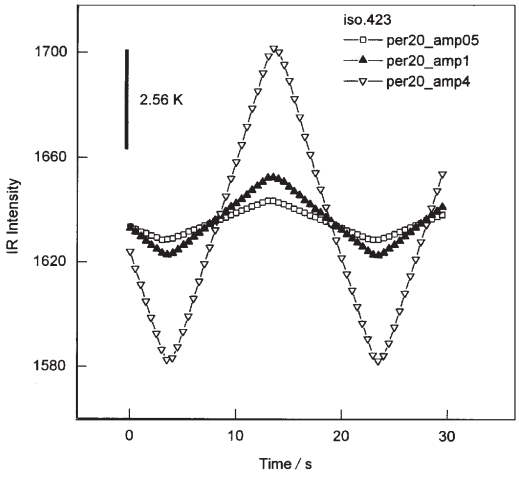

Fig. 3 Resolution of time and temperature of the infrared detector. Evaluation of a quasi-isothermal temperature modulation at 423 K, with a period of 20 s and amplitudes of 0.5, 1.0 and 4.0 K. The data were taken at the surface of the sample furnace

ticular case, *i.e.*, the selected sample-to-detector distance, lens and filter, is 33.3 intensity-units per Kelvin. When sample and reference sides were detected simultaneously by increasing the furnace-to-detector distance, a considerable, static temperature difference of the order of 1.0 K was measured as displayed in the insert in Fig. 2. This difference is attributed to the asymmetry of the instrument [15], and does not affect our experiments.

Figure 3 illustrates the temperature at the surface of the sample furnace in different modulation experiments as detected by the infrared camera. The figure permits to visualize the time and temperature resolution of the infrared camera. In this example, the period is 20 s and the programmed amplitudes are 0.5, 1.0 and 4.0 K. From the recorded single cycles, the minimum and maximum intensities were determined and converted into the temperature amplitudes A_{IR} , where the subscript IR denotes measurements with the infrared camera. Furthermore, we determined the amplitude at the sample sensor of the calorimeter, A_{T_s} , which is given by the calorimeter software. These two amplitudes, A_{IR} and A_{T_s} , are compared to the programmed amplitude, A_{T_p} by calculation of the normalized differences D_{IR} and D_{T_s} :

$$D_{IR} = \frac{A_{T_p} - A_{IR}}{A_{T_p}} \tag{3a}$$

$$D_{T_s} = \frac{A_{T_p} - A_{T_s}}{A_{T_p}} \tag{3b}$$

Results

For an empty sample furnace the deviations between the programmed temperature amplitudes, A_{T_p} , and the experimentally measured temperature amplitudes, A_{IR}, are plotted in Fig. 4 as function of the modulation period and heating rate (insert) after normalizing, as shown in Eq. (3a). Figure 4 also displays the analogous data for the sample-temperature amplitude A_{T_s} as indicated by the TMDSC, and expressed by Eq. (3b). First, one can see that the data recorded by the infrared camera and mea-

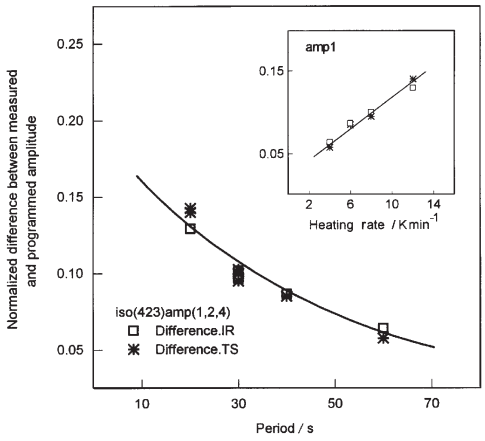

Fig. 4 Comparison between programmed and measured modulation amplitudes of the empty TMDSC furnace as function of the modulation period and heating rate, respectively (insert). (Period p=20 s shows data with amplitudes 1.0 and 2.0 K; p=30 s, 1.0, 2.0 and 4.0 K; p=40 s, 1.0 K; p=60 s, 1.0 K)

sured by the sample-temperature sensor of the TMDSC are identical within the error limit, *i.e.*, in this configuration there is only a negligible temperature gradient between the temperature sensor of the TMDSC and the surface of the empty sample furnace (Fig. 1b). Second, there is practically no influence of the programmed modulation amplitude of 1.0 to 4.0 K on the plotted deviation. Third, the data show a distinct dependence on the modulation period, p. The shorter the modulation period, *i.e.*, the higher the frequency, the larger is the lag behind the programmed amplitudes. Fourth, the insert of Fig. 4 shows that D_{IR} and D_{T_s} change linearly with heating rate. This result can be rationalized since p is directly linked to the (constant) heating and cooling

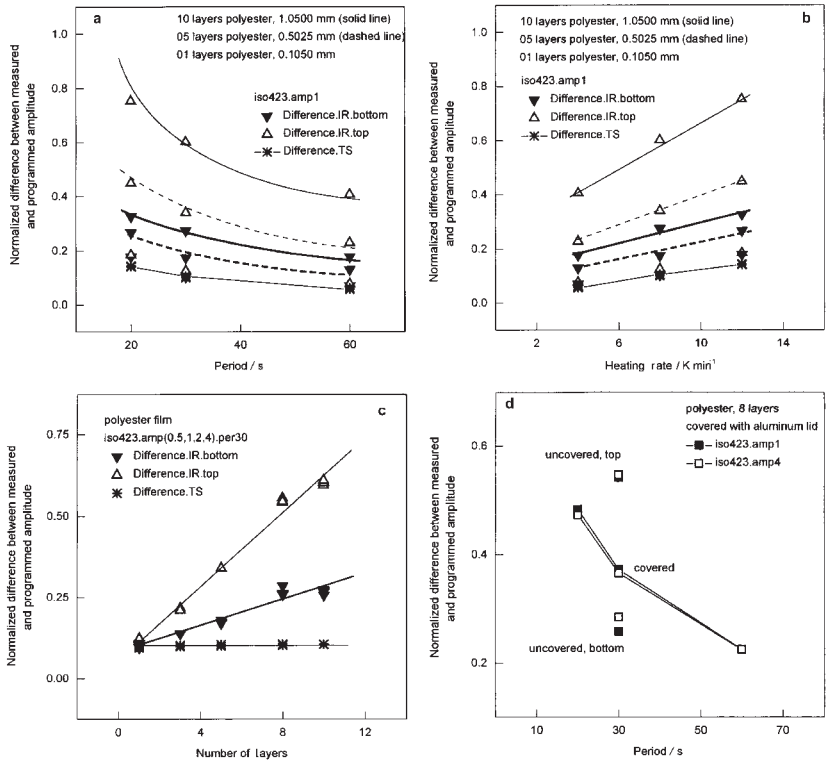

Fig. 5 Deviation between programmed and measured modulation amplitudes as given by Eq. (3a) of polyester films as function of the period, p, amplitude, A_{T_s}, heating rate, q, sample thickness, and covering of the sample with an aluminum lid
a Data measured at the top and bottom of the uncovered sample with A_{T_s} or A_{T_s}=1.0 K as a function of p
b Data as in 5a, but as a function of the heating rate, q
c Data similar to 5a, but with periods of 30 s and amplitudes from 0.5 to 4.0 K, as a function of sample thickness (one layer=0.105 mm)
d Data similar to 5a, but showing the influence of covering the sample by an aluminum lid on measuring at the top (solid lines), modulations with amplitudes of 1.0 and 4.0 K (■ and □, respectively)

rates, q, of the sawtooth modulation. At constant amplitude, A_{T_p}, a higher q results in a shorter p. An expression that connects p and q is given by: pq=240A_{T_p} (p in s, q in K min^{-1}). Since D_{IR} and D_{T_s} change linearly with q, they must change with the inverse of p. These small lags between programmed and actual temperature as expressed by Eqs (3a) and (3b) for the empty TMDSC must be due to an internal instrument lag between heater and sensor. They are described in their linear dependence on q by a relationship as seen in Eq. (1) where the C_p/K refers to a time constant of the sample furnace, and ΔT is the temperature difference between heater and temperature sensor.

Figure 5a shows the deviations between the programmed and measured amplitudes as function of the modulation period for the top (△) and bottom (▼) of the polyester samples of different thicknesses [about 0.1 mm (no lines), 0.5 mm (two dashed lines), and 1.0 mm (two upper solid lines)], together with reference data of Eq. (3b) (∗, bottom, thin solid line). Figure 5b contains the same data plotted *vs.* the heating rate, q, and Fig. 5c summarizes the influence of the sample thickness on the modulation amplitude. The effect of covering the sample with an aluminum lid is shown in Fig. 5d. Again, the plots of D_{IR} as functions of heating rate are linear.

Figure 6 represents data for poly(butylene terephthalate). In Fig. 7 the deviations between programmed and measured modulation amplitude are given for the liquid poly(ethylene-*co*-octene)s with a thickness of 0.175 and 1 mm.

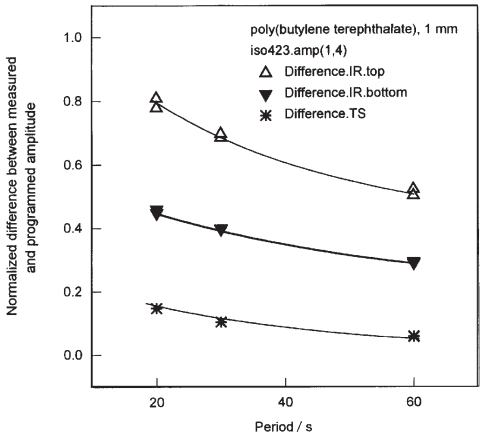

Fig. 6 Deviation between programmed and measured modulation amplitude as function of the period obtained at the top and bottom of a poly(butylene terephthalate) sample with a thickness of 1 mm. The differences of the program and sample temperatures are given by [∗, see Eq. (3b)]

All polymers reveal similar changes of the deviation between the programmed and measured modulation amplitude when the modulation period, *resp.*, the heating rate changes. With increased modulation period, the deviation decreases (Figs 5a, 6, 7). When data are plotted as function of the heating rate (Fig. 5b), the changes of the

measured amplitudes are linear, as was also shown in Fig. 4 with an empty calorimeter. The magnitude of the programmed amplitude, A_{T_p}, does not affect the results.

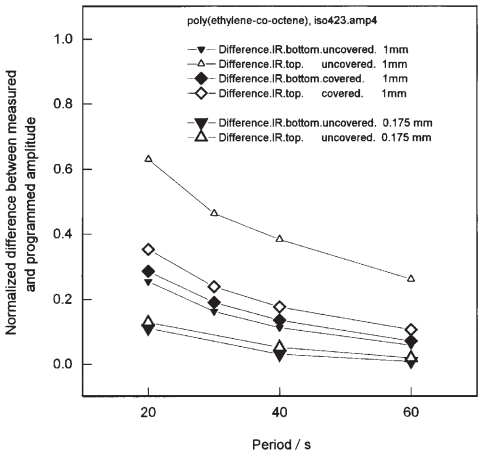

Fig. 7 Deviation between programmed and measured modulation amplitudes as function of the period obtained on liquid poly(ethylene-*co*-octene) (thickness 0.175 and 1 mm), covered and uncovered

The analyzed polymer samples, however, were prepared in such way that the infrared camera could simultaneously detect the surface of the sample and its bottom so that the temperature gradient within the sample could be assessed, as well as the temperature gradient between the sample-temperature sensor and the top of the furnace, as in Fig. 4, which is now identical to the temperature of the bottom of the sample. These experiments show significant differences from the empty furnace. The ampli-

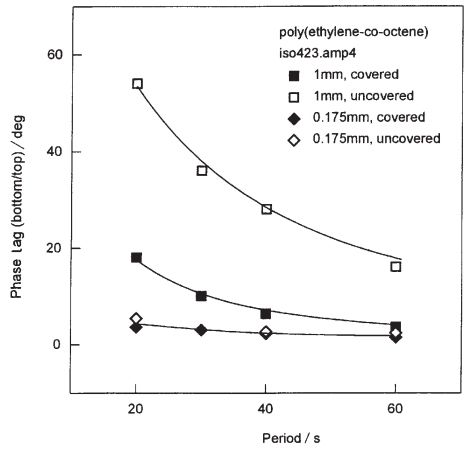

Fig. 8 Phase lag of modulation between bottom and top of covered and uncovered liquid poly(ethylene-*co*-octene) (thickness 0.175 and 1.0 mm) as function of the period

tude at the top of the uncovered sample, is considerably decreased when compared to the amplitude at the bottom of the pan, an effect that decreases with increasing modulation period. The deviations increase with the sample thickness at the top, as well as at the bottom (Fig. 5c). In case the samples are covered with an aluminum lid, the amplitudes at the top and bottom are almost equal (Fig. 7), but different from the empty furnace of Fig. 4. Figures 5 and 6 contain, for comparison, the amplitude deviation of the sensor temperature which is obviously the same for all experiments.

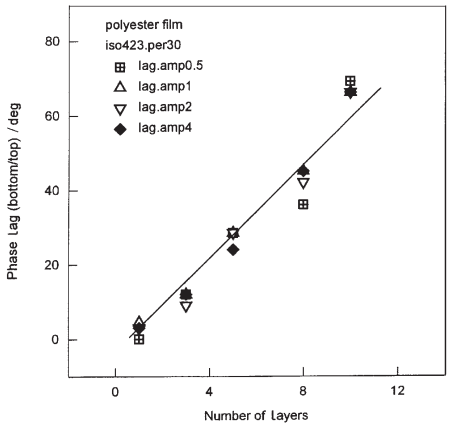

Fig. 9 Phase lag of modulation between bottom and top of the polyester film as a function of the sample thickness for different modulation amplitudes

Figure 8 summarizes the phase lag between the bottom and the top of the sample as function of the period for poly(ethylene-*co*-octene)s of different thicknesses, covered and uncovered with an aluminum lid, and Fig. 9 visualizes the dependence of the phase lag between the bottom and the top of the sample on the thickness of the polyester film.

Discussion

The experiments, which are described above, were performed to reveal the temperature gradients in typical polymer samples as functions of the modulation parameters, sample thicknesses and experimental setup, *i.e.*, the path of heat delivery into the sample. The parameters of the quasi-isothermal sawtooth modulation were varied from 0.5 to 4 K in amplitude and 20 to 60 s in period, resulting in heating rates between 1 and 48 K min^{-1}. The sample thickness was systematically changed from 0.1 to 1 mm. Furthermore, the surface temperature of the samples was measured when the sample was not covered with an aluminum lid, and in the presence of an aluminum lid. In addition to the evaluation of the temperature gradient, we estimated the phase lag of the modulation through the sample.

First, it was possible to verify that there is no measurable difference between the amplitudes of the sensor temperatures as recorded by the DSC and the actual surface temperature of the sample furnace as long as it contains no sample, but there exists a

temperature difference between the heater and the sensor temperature that increases linearly with q (Fig. 4). Since the sensor temperature is involved in the control of the modulation [11], its amplitude does not depend on the sample properties, including the sample mass, *i.e.*, D_{T_s} of Eq. (3b) remains constant in Fig. 5c and depends only on the modulation parameters, as is shown for the empty furnace in Fig. 4 and with different samples in Figs 5a, b, and 6. It is interesting to note that the control of T_s does not lead to $D_{T_s}=0$, as one finds for heat-flux calorimeters with control at T_s. This measurement cannot be discussed further, as long as the Perkin Elmer control of the DDSC is not disclosed in detail, but must be taken as an empirical measurement of the temperature gradient between heater and T_s.

In contrast to D_{T_s}, the normalized difference between the amplitudes of the programmed and actual sample-surface temperature, the D_{IR} of Eq. (3a), changes with the properties of the sample, as expected for the given setup with the heater located underneath the sample and sample-temperature sensor. The amplitude at the surface decreases with increasing sample thickness, as is seen in Figs 5a–c and 7 (Δ). In particular, Fig. 5c illustrates the dependence of D_{IR} on the sample thickness. For the samples of 1 mm thickness at a p of 30 s in Figs 5a, 6, and 7, the programmed amplitudes have decreased at the top of the sample surfaces to 60, 69, and 46%, respectively (open triangles). The different results for the different polymers must be caused by different heat-transfer conditions, but will not be discussed further, albeit the fact that these types of experiments might be used to extract thermal conductivities of the samples. However, at this moment we want to treat all samples as polymers, not distinguishing further with respect to their thermal diffusivity. When the thickness of the sample gets sufficiently low, *i.e.*, reaches about 0.1 mm, the amplitude of the temperature at the surface becomes close to that of the sensor (Figs 5a–c). Under the most extreme modulation conditions used in this research, *i.e.*, a programmed amplitude of 4.0 K with a period of 20 s which leads to heating and cooling rates of 48 K min^{-1}, the measured amplitudes at the bottom and the top of 1 mm thick poly(ethylene-*co*-octene) are 2.98 and 1.48 K, respectively; compared to 3.56 and 3.49 K for the 0.175 mm sample (Fig. 7).

A simple one-dimensional heat-flow model can be used to understand this result. Assuming heat is introduced across a surface of uniformly modulated temperature into the bulk of a sample, the decrease of the maximum temperature amplitude, A, as a function of the distance, x, from the surface can be calculated with [16]:

$$A(x)=A(0)\exp\left[-x\sqrt{\frac{\pi}{kp}}\right] \tag{4}$$

where $A(x)$ and $A(0)$ are the amplitudes at the layer at distance x in mm from the surface and at the surface (x=0 mm), respectively; k is the thermal diffusivity in mm^2 s^{-1}; and p the period in s, as before. Using different thermal diffusivities k of 0.2, 0.3, and 0.4 mm^2 s^{-1} in Eq. (4), which are reasonable for polymers, one approaches a fit to our experimental data, as is depicted in Fig. 10. We need to point out that we used the

measured amplitude at the bottom of the sample as $A(0)$ (*via* infrared thermography), and neither the programmed amplitude nor the amplitude of the sensor temperature.

The amplitude-differences at the bottom of the samples are much less than at the top of the sample (▵), as expressed by Eq. (3a) (▾ in Figs 5a–c, 6 and 7). The overall temperature gradients between the heater and sensor, the sensor and surface temperature, and the surface temperature and top of the sample are caused by the presence of the sample. Without a sample, only the relatively small gradient between the heater and the sensor remains ($T_s=T_{IR}$ at the furnace surface, Fig. 4). This explanation is sup-

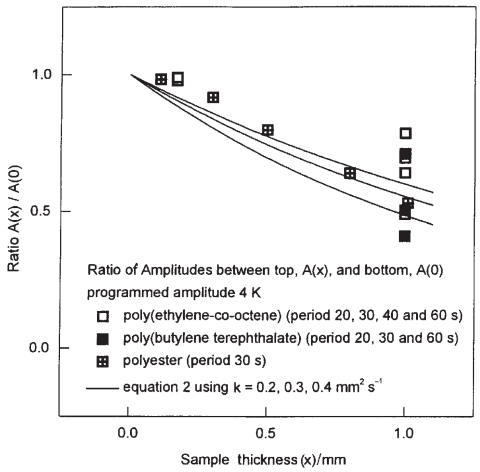

Fig. 10 Normalized decrease of the modulation amplitude *vs.* sample thickness; experimental data and fit by Eq. (2)

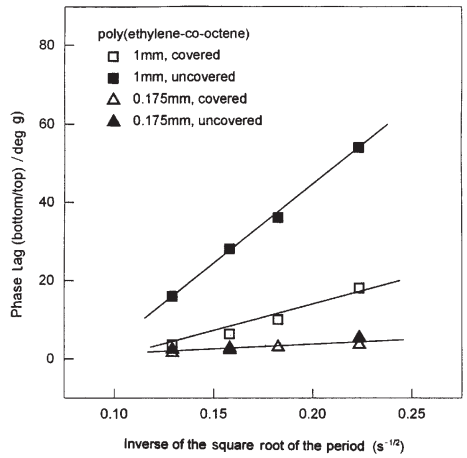

Fig. 11 Phase lag of modulation between bottom and top of covered and uncovered poly(ethylene-*co*-octene) (thickness 0.175 and 1.0 mm) as function of the inverse of the square root of the period ($p^{-1/2}$)

ported by the fact that for covered samples the differences between top and bottom almost disappear, and, more importantly, their amplitudes are between that of the uncovered sample, measured at the top and at the bottom (Figs 5d and 7). In this case, the heat preferentially flows along the path of lower thermal resistance, along the sides of the aluminum pan to the lid, rather than through the polymer sample, and almost half of the heat needed to modulate the sample flows through the top cover. By reducing the decrease of the amplitude at the top of the sample, the total heat flow into the sample is increased, which in turn increases the gradient between T_s and T_{IR} at the furnace surface, caused by the larger heat flow.

A similar reasoning can be applied to the changes in phase angle ϕ shown in Figs 8 and 9. Using the same one-dimensional heat-flow model, one can calculate the phase angle $\phi(x)$ at position x as [16]:

$$\phi(x)=180x\sqrt{\frac{1}{pk\pi}} \tag{5}$$

According to Eq. (5) one expects a linear increase in the phase lag between the bottom and top of the sample when plotting $\phi(x)$ *vs.* the inverse square root of the period, as it is done for the poly(ethylene-*co*-octene) sample in Fig. 11. The experimental data fit the expected relation as illustrated in Fig. 11. Similar to Fig. 10, Fig. 12 is a plot of Eq. (5) with thermal diffusivities k of 0.2, 0.3, and 0.4 $mm^2\ s^{-1}$, compared to our experimental values.

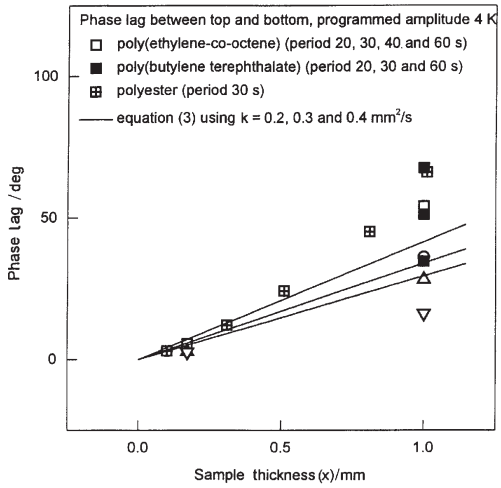

Fig. 12 Phase lag of modulation between bottom and top of the polyester film as function of the sample thickness; experimental data and fit by Eq. (3)

Figure 13, finally, depicts a calculation of the temperature amplitude $A(x)$ from the bottom of the sample (position 0) to the position x as a function of time t [16]:

$$A(x)=A(0)\exp\left[-x\sqrt{\frac{\pi}{kp}}\right]\cos\left(x\sqrt{\frac{\pi}{kp}}-\frac{2\pi}{p}t\right) \quad (6)$$

The exponential term is the reduction of the maximum amplitude with increasing penetration depth x and the cosine-term contains the phase shift *vs.* x and the time dependency. The data in Fig. 13 were calculated using the experimentally determined amplitude reductions at the bottom of the uncovered 1 mm thick poly(ethylene-*co*-octene) sample which is 2.98 K (programmed amplitude 4 K, period 20 s). If the sample is covered, there is additional heat input from the top cover. This increases the amplitudes towards A_{T_p} and changes the phase shift, as shown by the experimental data of Figs 5d and 8. A calculation of the small difference between the heat input from the bottom and the top requires more accurate experimental data, as well as the calculation of thermal conductivity from the data of Fig. 12 may need more accurate results to separate instrument- from sample-effects.

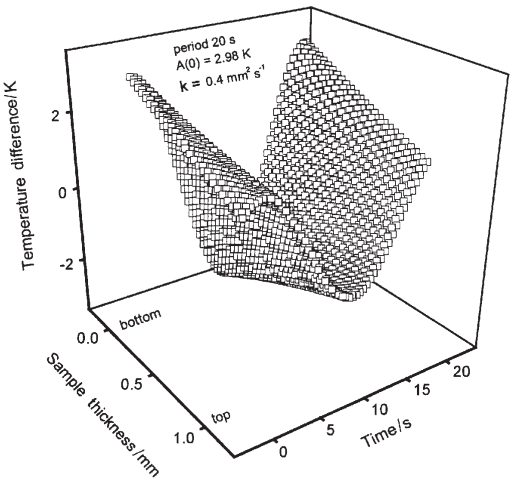

Fig. 13 Modulated temperature as function of sample position and time, calculated using Eq. (6)

A first step to these more involved calculation may be based on the model of Buehler *et al.* [13, 14]. At present these calculations are unnecessarily simplified by describing a cylindrical sample which has one of the two flat surfaces without heat flow, and assumes a constant temperature at the other flat surface and the sides. This could easily be adapted to the case of a fully enclosed sample with constant temperatures all-around which would produce a mirror-plane at the center without heat-flow and correspond to double the assumed model. Without further complications such model would correspond to the experiments described in this paper.

Conclusions

With the high-speed, high-sensitivity infrared camera, direct measurements were made of the temperature gradients inside a TMDSC between the heater and sensor, the sensor and surface temperature, and the surface temperature and top of the sample as they are caused by the presence of the sample. Without a sample, only a relatively small gradient between the heater and the sensor remains. The temperature gradients are inversely proportional to the modulation period and linearly proportional to the heating rate. In samples completely surrounded and contacted by the aluminum pan, the top and bottom surfaces of the sample are practically at the same temperature, and close to half of the heat flow into the sample goes through the top surface. A simple, one-dimensional heat-flow model is in accord with the general appearance of the data. More detailed calculations should be possible when using the three-dimensional model of Buehler *et al.* Finally, the data indicate that multifrequency measurements, as developed recently may in the future also be used for measurement of both, C_p and k in a single experiment by proper interpretation of the constant τ which is used for correction of Eq. (2) [9].

* * *

This work was supported by the Division of Materials Research, National Science Foundation, Polymers Program, Grant # DMR-9703692 and the Division of Materials Sciences, Office of Basic Energy Sciences and the Office of Transportation Technologies, as part of the High Temperature Materials Laboratory User Program, U.S. Department of Energy at Oak Ridge National Laboratory, managed by Lockheed Martin Energy Research Corp. for the U.S. Department of Energy, under contract number DE-AC05-96OR22464.

References

1 B. Wunderlich, Thermal Analysis, Academic Press, New York 1990; see also, Differential Thermal Analysis, in Physical Methods of Chemistry, A. Weissberger and B. W. Rossiter, eds. Vol. 1, Part V, Chapter 8, pp. 427–500. John Wiley & Sons, Inc., New York 1971; The Basis of Thermal Analysis, in Thermal Characterization of Polymeric Materials, E. Turi, ed. Vol. 1. Chapter 2, pp. 205-482, Academic Press, second edition, New York 1997; all are updated and expanded in the computer-based course: Thermal Analysis of Materials, which can be downloaded from the Internet, including the presentation software at the following address: web.utk.edu/~athas/courses/tham99.html

2 H. Wang, M. Bartkowiak, F. A. Modine, R. B. Dinwiddie, L. A. Boatner and G. D. Mahan, J. Am. Ceram. Soc., 81 (1998) 2013.

3 A. Mehta, R. C. Bopp, U. Gaur and B. Wunderlich, J. Thermal Anal., 13 (1978) 197.

4 B. Wunderlich, Y. Jin and A. Boller, Thermochim. Acta, 238 (1994) 277; A. Boller, Y. Jin and B. Wunderlich, J. Thermal Anal., 42 (1994) 307.

5 B. Wunderlich, A. Boller, I. Okazaki, K. Ishikiriyama, W. Chen, M. Pyda, J. Pak, I. Moon and R. Androsch, Thermochim. Acta, 330 (1999) 21.
6 T. Ozawa, Bull. Chem. Soc., Japan, 39 (1966) 2071.
7 R. Androsch, I. Moon, S. Kreitmeier and B. Wunderlich, Thermochim. Acta, in press (2000).
8 R. Androsch and B. Wunderlich, Thermochim. Acta, 333 (1999) 27.
9 B. Wunderlich, R. Androsch, M. Pyda and Y. K. Kwon, Thermochim. Acta, 348 (2000) 181.
10 Y. K. Kwon, R. Androsch, M. Pyda and B. Wunderlich, Thermochim. Acta, accepted (Perkin Elmer DSC); M. Pyda, Y. K. Kwon and B. Wunderlich, Thermochim. Acta, accepted (TA Instruments DSC); J. Pak and B. Wunderlich, Thermochim. Acta, accepted (Mettler-Toledo DSC). See also Proc 27th Natas Conference in Savannah, GA Sept. 19–22, 27 (1999) 339 and 345.
11 J. E. K. Schawe and W. Winter, Thermochim. Acta, 298 (1997) 9.
12 M. Reading, B. K. Hahn and B. S. Crowe, U. S. Patent, Method and Apparatus for Modulated Differential Analysis, 5,224,775, July 6, 1993.
13 F. U. Buehler, C. J. Martin and J. C. Seferis, Proc. 26th NATAS Conf. in Cleveland, OH, Sept. 13–15, 1998, K. R. Williams, Ed., 26 (1998) 44.
14 F. U. Buehler and J. C. Seferis, J. Therm. Anal. Cal., 54 (1998) 1.
15 J. E. K. Schawe, private communication at the 26th NATAS Conference. in Cleveland, OH, Sept. 13–15, 1998.
16 H. Gröber and S. Erk, Fundamentals of Heat Transfer, McGraw-Hill 1961, pp. 77–89.